Rev. Adv. Mater. Sci. 49 (2017) 140-149

CARBON COMPOSITES AS ANODE MATERIALS FOR LITHIUM-ION BATTERIES

I.A. Stenina[1], T.L. Kulova[2], A.M. Skundin[2] and A.B. Yaroslavtsev[1]

[1]Kurnakov Institute of General and Inorganic Chemistry, Russian Academy of Sciences, Leninsky pr. 31, Moscow, 119991, Russia
[2]Frumkin Institute of Physical Chemistry and Electrochemistry, Russian Academy of Sciences, Leninsky pr. 31, Moscow, 119991, Russia

Received: July 10, 2016

Abstract. Anode materials based on silicon, tin, titanium oxides and lithium titanate, as well as their composites with carbon for lithium-ion batteries are reviewed. A large change in volume upon lithium intercalation-deintercalation results in fast degradation of anode materials based on silicon and tin. Formation of nanocomposites with carbon allows to stabilize these materials and their cycling performance. The processes of carbon coating formation are considered in more detail for lithium titanate, a promising anode material, as an example. In this case, carbon ensures acceleration of diffusion across the grain boundaries. The effect of the temperature treatment and the carbon precursor on the formation and electrochemical properties of a composite material based on $Li_4Ti_5O_{12}$ and carbon is considered. It is shown that the size of $Li_4Ti_5O_{12}$ particles can be controlled by the amount of the carbon precursor and the calcination temperature. The combination of data of X-ray powder diffraction, thermogravimetry, Raman spectroscopy, and electrochemical testing shows that formation of a conductive carbon coating requires preliminary sample heating in air at temperatures no lower than 400°C followed by calcination in an inert atmosphere.

1. INTRODUCTION

Lithium-ion batteries (LIB) have become popular as power sources in today's mobile communication devices, notebooks, digital photo and video cameras, vehicular transport, etc. The main reason is that they have high power capacity and reliability [1]. The LIB operation is based on processes of lithium intercalation and deintercalation in cathode and anode materials. The power capacity of a battery is determined by the potential difference of these processes and the electrochemical capacity of these materials [2]. On the other hand, the main problems of LIB development are related to the development of new electrode materials. Imperfection of these materials considerably limits their use in a number of potential applications. For example, increasing the power and charge/discharge rates of batteries is quite an important task. A few approaches are used to solve this problem. They are based on doping with heterovalent ions, as well as transition to nanosized materials, nanocomposites, primarily with carbon [3]. The main aim of this publication is to make a brief overview of data on the use of nanocomposites with carbon as anode materials and a more detailed discussion of such composites for lithium titanate.

2. ANODE MATERIALS BASED ON CARBON, SILICON AND TIN

Most often, graphite is used as an anode material in LIB. It is characterized by high charge and dis-

Corresponding author: A.B. Yaroslavtsev, e-mail: yaroslav@igic.ras.ru

charge rates. Furthermore, it has a relatively high theoretical capacity (372 mAh/g), which is determined by reversible lithium intercalation into the interplanar space [4]. The low working potential (0.15-0.25 V) ensures a high power capacity of batteries. However, the volume change during charge/discharge results in fast degradation of graphite anodes, especially at high current densities.

The charge and discharge rates of electrodes in lithium-ion batteries is predominantly determined by the diffusion of lithium ions and the electronic conductivity of electrode materials. Their charge and discharge times are proportional to the square of the diffusion layer thickness. Diffusion by grain boundaries usually occurs much more quickly than in crystals [5]. Therefore, the rate of electrochemical processes is highly determined by the particle size. The charge and discharge rates of a battery are the higher, the smaller the crystal size of the electrode material. In view of this, high expectations were placed in the use of carbon nanomaterials. However, lithium is incorporated into carbon nanotubes only through the end faces [58]. Therefore, the diffusion layer thickness for these processes is rather high, while the material capacity is comparatively low [6-10].

In other carbon nanomaterials, including nanofibers, graphene and thermally expanded graphite, lithium binding at low potentials only occurs on the outer surface. Therefore, the electrode potentials of lithium intercalation and deintercalation differ considerably and vary in a broad voltage range (usually from 0 to 3 V). In this case, charging the battery requires much more power than the amount released upon discharging. Moreover, the capacity of carbon nanomaterials at low potentials that are of interest for lithium-ion batteries is considerably lower than the capacity of graphite [11]. A considerable drawback of all carbon nanomaterials for lithium-ion batteries is that they have a high irreversible capacity during the first charge and discharge cycles [12,13].

Silicon has a record-high theoretical capacity for lithium intercalation (4200 mAh/g). Unfortunately, this process is accompanied by a fourfold increase in the unit cell volume [14] resulting in degradation of the anode material [3]. After as little as ten cycles, the capacity of the anode material decreases to 200 mAh/g [15]. This problem is solved by using thin-film electrodes made of amorphous silicon [16-19]. The effect is reached due to material disordering and possibility of expansion in a direction perpendicular to the film orientation. The cyclic performance of amorphous silicon films decreases with an increase in thickness [20,21]. However, the use of thin-film electrodes complicates the battery design considerably. A better effect is achieved by using high-porosity samples and nanoparticles [22-26], including whiskers [27,28] and “core in shell” structures [29,30]. For example, nanoparticles of 5 nm in size were obtained, the capacity of which remained at 2500 mAh/g for more than 40 cycles [31].

Tin presents properties similar to those of silicon. Its intermetallide with the maximum content of lithium is $Li_{4.4}Sn$. It corresponds to a theoretical capacity of about 990 mAh/g [32]. However, in this case lithium intercalation is also accompanied by a 3 – 3.5 fold volume increase [33]. As a result, the anode already deteriorates during the first cell charging. The material is stabilized if nanosized particles are used [34]. In fact, electrodes based on tin nanowhiskers have a capacity of 400 mAh/h and show a good cyclic performance [35].

Tin alloys with some other metals are more stable [36]. For example, the theoretical capacities of $FeSn_2$ and $FeSn_5$ intermetallides are 500 and 750 mAh/g, respectively [37], whereas those of tin-antimony alloys are up to 600 mAh/g [38]. Fairly good results are obtained with tin alloys in the form of thin-film electrodes [39,40]. It should be noted that lithium deintercalation in such systems occurs at higher potentials, thus decreasing the battery efficiency.

3. COMPOSITES OF SILICON AND TIN WITH CARBON

Creation of composites of silicon and tin with carbon [41-45] is a promising approach. A significant advantage of carbon is that it has high electric conductivity and provides fast lithium transfer. Therefore, incorporation of carbon results in high rates of lithium transfer by grain boundaries. Furthermore, carbon nanomaterials ensure binding between nanosized particles of other materials and stabilize them. In fact, the capacity of composite anode materials based on silicon and carbon changed from 1040 to 790 mAh/g during the first 20 cycles [46].

High-porosity composites of silicon and carbon showed an even higher capacity of 1950 mAh/g that is close to the theoretical value [47]. Capacity of 1200 - 1500 mAh/g was obtained for composites of silicon nanoparticles with graphene [48, 49]. On the other hand, the capacity of silicon composites with carbon nanotubes was considerably lower [50]. Studies on preparation of layered silicon-carbon composites by means of magnetron sputtering deserve special attention [51].

Appreciable success was also reached for composites of tin with carbon materials. For example, nanocomposites show a capacity of 500 mAh/g for 200 cycles [52]. A capacity of about 600 mAh/g after 200 cycles was obtained for composites of carbon with a tin-iron alloy [53]. The capacity of an anode material based on tin nanoparticles in a carbon shell was 760 mAh/g [54]. Studies on carbon composites with tin alloys with copper and nickel [55,56] and tin with carbon nanotubes [57,58] are also worth noting.

4. TITANIUM OXIDES AND LITHIUM TITANATE

A number of studies deal with the use of titanium oxide as an anode material for LIB. Lithium intercalation results in formation of Li_xTiO_2 phase containing tri- and tetravalent titanium ions. Lithium intercalation into anatase, which shows the best properties, results in phase separation into a Li-rich ($Li_{0.55}TiO_2$) phase and Li-poor ($Li_{0.01}TiO_2$) phase [59,60]. As a result, lithium intercalation and deintercalation occur at a nearly constant potential (1.72-1.75 V for lithium intercalation and 1.8-1.9 V for lithium deintercalation). The volume change in these processes is as small as 4% [61]. Intercalation of lithium into rutile occurs in a similar way. The composition of the lithium-rich phase is $Li_{0.5}TiO_2$, but the structure changes more considerably in this case [59,62]. Due to the low electric conductivity of titanium dioxide, it is always used in nanomaterials or their composites with carbon. It has been shown that smaller anatase particles can be electrochemically reduced to $LiTiO_2$, though the capacity does not exceed 200-230 mAh/g even in the first cycles [63-66], which indicates that a considerable Ti^{4+} ions fraction remain in initial form. The use of anatase composites with carbon nanotubes [67] and with graphene [68] was reported. Similar results were obtained for composites of rutile-TiO_2 with carbon [69]. An initial capacity of 380 mAh/g was obtained for composites based on its whiskers [70].

At the same time, lithium titanate $Li_4Ti_5O_{12}$ attracts much more attention. Its composition can be presented as $Li[Li_{1/3}Ti_{5/3}]O_4$, which shows that a part of lithium is located in titanium positions, while lithium occupies both octahedral and tetrahedral sites. This material can accept one more lithium ion per formula unit, which corresponds to a theoretical capacity of 175 mAh/g [71,72]:

$$Li_4Ti_5O_{12} + 3e^- + 3Li^+ = Li_7Ti_5O_{12} \quad (1)$$

The lithiated and delithiated forms have very low mutual solubility, and the coexisting compositions correspond to the $Li_{6.93}Ti_5O_{12}$ and $Li_{4.03}Ti_5O_{12}$ formulas [73]. Therefore, the charge and discharge occur at a nearly constant potential of 1.55 V. It should also be noted that the cubic lattice parameter of these materials differ by less than 0.1% (8.3595 and 8.3538 Å) [74]. This determines the high cycling stability of the material.

The main drawback of lithium titanate is low electronic (10^{-12} - 10^{-13} S/cm) and lithium ($3\cdot10^{-10}$ S/cm) conductivities [75,76]. For this reason, lithium titanate is commonly used as nanomaterials [77-80].

5. COMPOSITES OF LITHIUM TITANATE WITH CARBON

The main approach for increasing the electronic conductivity of $Li_4Ti_5O_{12}$ is to create composite materials with a highly conductive phase, such as Ag [81] or polyacenes [82]. However, composite materials based on lithium titanate and carbon, including carbon black, graphene, carbon nanotubes, etc., are studied more commonly [83-88].

For carbon coating, a carbon precursor and lithium titanate mixture is calcined at high temperatures in an inert or reducing atmosphere. As carbon sources sucrose, glucose, starch, and various organic acids are used most commonly [89,90]. It was suggested to use phenanthroline as a carbon precursor [91]. The resulting material showed a capacity of 145 mAh/g at 10 C with retention of 96.6% after 100 cycles. (The cycling rate *X*C corresponds to complete cell charging in 1/*X* hours). According to [92], the electrospinning method with polyvinylpyrrolidone as the carbon source is promising for creation of commercial anodes. The CVD method was also used to create a carbon coating [93,94].

The resulting carbon coating is not always uniform. It is believed [95] that the electronic conductivity of such nanocomposites of lithium titanate and carbon is reduced due to the lack of reliable contacts between particles. It is believed that the problem might be solved by creating more complex composite materials, including lithium titanate, carbon black, and carbon nanotubes that act as some kind of bridges. In fact, at 5C, the capacity of the materials obtained, namely, $Li_4Ti_5O_{12}$, $Li_4Ti_5O_{12}$/C and $Li_4Ti_5O_{12}$/C/CNT, was 100, 132 and 148 mAh/g, respectively [95]. It is most promising to obtain composites of lithium titanate with carbon using an organic salt of lithium as a source of both lithium and carbon. In this case, an additional stage of mixing a carbon precursor with lithium titanate is excluded,

Table 1. Sizes of $Li_4Ti_5O_{12}$ and TiO_2 (anatase) particles in the materials studied, estimated from the broadening of X-ray diffraction lines (CSR).

Thermal treatment conditions		Particle size, nm	
		$Li_4Ti_5O_{12}$	TiO_2 (anatase)
Temperature of calcination in air, °C	400	4.0	5.3
	600	43	54
	800	Reference sample	-
Temperature of calcination in argon,	600	25	40
°C, after pre-treatment in air at 400 °C	600*	16	25
	800	130	-
	800*	83	-

*With addition of 8 wt.% sucrose

while the resulting carbon coating is more uniform. For example, an alternative method was suggested for synthesizing carbon-incapsulated lithium titanate by lithium acetate pyrolysis [96]. The capacity of the obtained material increases up to 134.7 mAh/g at 600 mA/g. Lithium lactate was also used for this purpose [97]. The capacity of the resulting material was 140 mAh/g at 10 C, with 90.2% efficiency after 200 cycles.

6. INVESTIGATION OF COMPOSITES OF LITHIUM TITANATE WITH CARBON

Nanocomposites of lithium titanate with carbon were synthesized using the sol gel method, from titanium tetrabutoxide and lithium carbonate in the presence of citric acid. The precursor obtained after pyrolysis at 250 °C for 5 h was heated at 400 °C for 5 h in air and calcined finally at 400, 600, and 800 °C for 5 h in a argon flow, with or without addition of 8 wt.% sucrose.

X-Ray analysis of samples was carried out with a Rigaku D/MAX 2200 diffractometer, CuK_α radiation. The spectra were processed using the Rigaku Application Data Processing software package.

The microstructure of samples was analyzed with a Carl Zeiss NVision 40 scanning electron microscope. Transmission electron microscopy was carried out with a Jeol JEM 2100 microscope, accelerating voltage 200 kV.

Thermogravimetric analysis was performed using a Netzsch TG 209 thermobalance in platinum crucibles in air, followed by analysis of the gas phase composition by means of an Aeolos QMS 403C mass spectrometer. The temperature range was 25-800 °C, the heating rate was 10 K/min, the sample weights were 20-30 mg.

Raman spectra were recorded with a LabRAM 300 HORIBA-Jobin Yvon instrument with excitation by the 632.8 nm of a He-Ne laser; the radiation power was 1 mW.

Absorption IR-spectra were recorded using an FT-IR NEXUS spectrometer (Nicolet).

The electrochemical characteristics of lithium titanate – carbon nanocomposites were studied in sealed three-electrode electrochemical cells with a lithium counter electrode and a lithium reference electrode. The working electrodes were made using the standard casting technology. A stainless steel mesh was used as the current collector. The active material was prepared by mixing a nanocomposite powder, carbon black (Timcal), and polyvinylidene fluoride (Aldrich) preliminarily dissolved in N-methylpyrrolidinone (Aldrich). The amount of the active compound on the electrode was about 10–15 mg/cm^2. Electrodes were compressed under 1000 kg/cm^2 pressure, followed by drying *in vacuo* at 120 °C. Electrochemical cells were assembled in a glove box with a dry argon atmosphere. An 1 M $LiPF_6$ solution in an ethylene carbonate – diethyl carbonate – dimethyl carbonate mixture (1:1:1) was used as the electrolyte (all the electrolyte components were of "extra dry" grade, Aldrich). Nonwoven polypropylene 25 mm thick was used as the separator.

If calcination is performed in air, formation of the $Li_4Ti_5O_{12}$ phase begins already at 400 °C; the X-ray pattern also contains reflexes of anatase-TiO_2 (Fig. 1). The particle size of these phases (coherent scattering region (CSR)), estimated from the Debye-Sherrer equation, is of 4 and 5 nm, respectively (Table 1). Subsequent calcination of this sample in the inert atmosphere at 400 °C does not change the X-ray pattern appreciably. At the same time, increasing the calcination temperature to 600 °C results in considerable narrowing of reflexes due to a

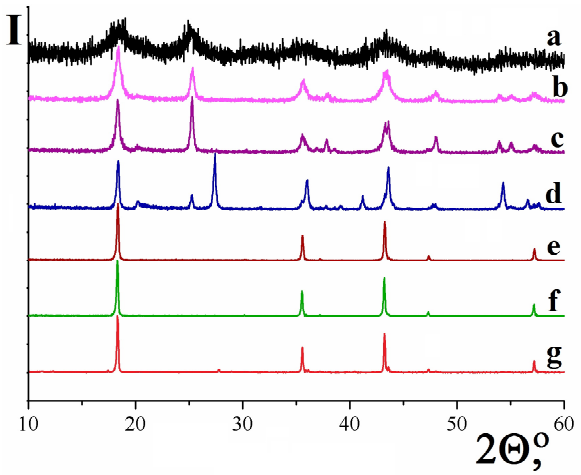

Fig. 1. X-ray diffraction patterns of the samples calcined in air at 400 (a), 600 (d), 800 °C (g), in the inert atmosphere at 600 (b, c), 800 °C (e, f) without (c, f) and with addition of 8 wt.% sucrose (b, e).

growth of $Li_4Ti_5O_{12}$ and anatase particles (Fig.1, Table 1). This effect is more significant for the latter. It should be noted that in samples calcined in air, a considerable fraction of titanium oxide is represented by rutile, whereas the X-ray patterns of the materials obtained in the inert atmosphere only contain anatase reflexes. The CSR of $Li_4Ti_5O_{12}$ in the samples obtained with addition of sucrose before the final calcination is much smaller (Table 1) due to formation of a more developped carbon coating that prevents particle growth. It can also be noted that the X-ray patterns of materials obtained without sucrose addition show the presence of considerable Li_2TiO_3 amounts (Fig. 1). After calcination at 800 °C, both in air and in the inert atmosphere, the X-ray patterns of the materials obtained show only reflexes of lithium titanate. However, it can be noted again that the materials obtained in the inert atmosphere are characterized by smaller particle size (Table 1), in agreement with SEM data (Fig. 2). Thus, it can be concluded that the particle sizes of lithium titanate and anatase are affected by both the final calcination temperature and addition of sucrose before the final calcination in the inert atmosphere.

According to transmission electron microscopy data, the materials obtained at 400 °C have the form of a layered polycrystalline compound with particle size ranging within 3-8 nm, in which the distance between atom layers corresponds to various lattice spacings of $Li_4Ti_5O_{12}$ and anatase, as also confirmed by the ring positions in the electron diffraction spectra. On increasing the calcination temperature to 600 °C, the particle size increases to 10 – 100 nm (Fig. 3a), while the electron diffraction patterns con-

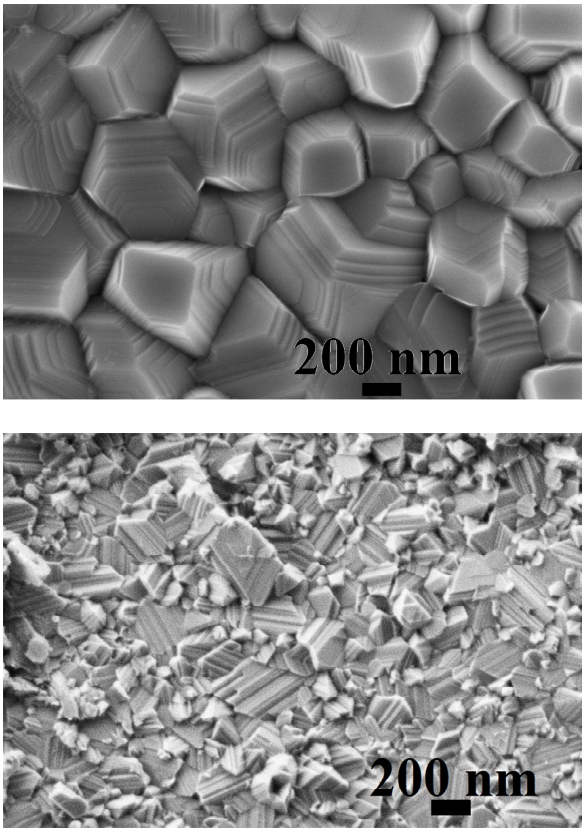

Fig. 2. SEM images of samples calcined at 800 °C in air (a) and in the inert atmosphere with sucrose addition (b).

tain, in addition to the rings, a considerable number of point reflexes corresponding to specific orientations of individual crystals. In this case, the particles obtained without sucrose addition before the final calcination are markedly larger, in agreement with XRD data. The particles are coated with an amorphous carbon phase, 2-3 nm thick for particles obtained without sucrose addition and 8-10 nm thick for particles obtained with sucrose addition before final calcination. The size of particles obtained at 800 °C is 150-200 nm; the distances between the atomic layers mainly agree with those for (111) reflexes of $Li_4Ti_5O_{12}$ and (103) reflexes of anatase (Figs. 3b-3d).

According to data of thermogravimetry with mass spectrometry of evolved gases, thermolysis of samples obtained at 400 and 600 °C occurs in three stages. At the first stage (25-280 °C), loss of water and carbon dioxide sorbed on the developed material surface is observed. The smaller the particles, the greater the mass loss. At the second (280-450 °C) and third stages (above 450 °C), only

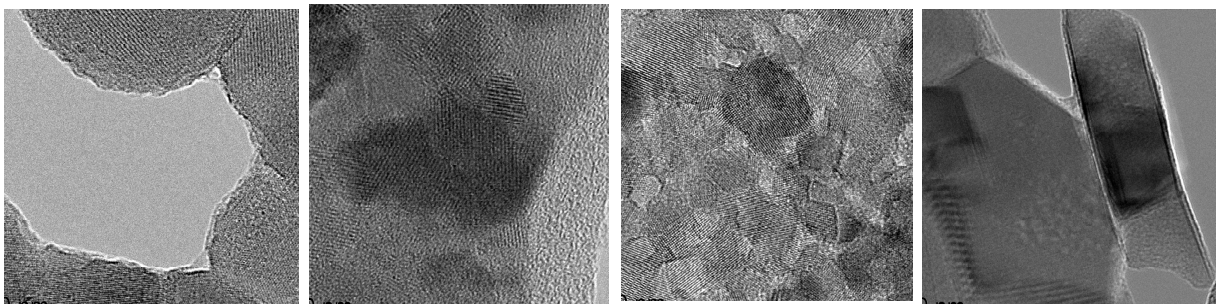

Fig. 3. TEM images of samples calcined in an inert atmosphere at 600 (a-c) and 800 °C (d) without (a) and with sucrose addition (b-g).

CO_2 is evolved due to burning of organic compounds and carbon. In the case of calcination in the inert atmosphere at 800 °Ñ, the total mass loss is very small and separate stages cannot be distinguished. The carbon content in materials calcined at 600 °C in the inert atmosphere with sucrose addition is of 2-3%. It decreases to 0.5-1% as the temperature is increased to 800 °C. Furthermore, the carbon content in the final product nonlinearly depends on the amount of sucrose added.

The IR-spectra of materials obtained at 400 and 600 °C in the inert atmosphere contain bands in the 740-870 and 1030-1110 cm^{-1} regions corresponding to vibrations of C-H and C-O-C bonds, which indicates incomplete sucrose carbonization. On increasing the calcination temperature to 800 °C, these bands disappear gradually, and the most intense absorption is observed in the 1524 and 1423 cm^{-1} ranges characteristic of graphite C-C bonds. To study the structure of the carbon coating obtained, we recorded Raman spectra in the 900-2000 cm^{-1} range (Fig. 4). The spectra of materials obtained at 400 °C in air are characterized by a very high background, therefore specific absorption of could not be separated. In the spectrum of a sample calcined in the inert atmosphere at 400 C, it is possible to distinguish at least 5 peaks (Fig. 4a) corresponding to carbon fragments with different structures. In fact, absorption at 1580 cm^{-1} (D band) is characteristic of single-crystalline graphite phase (sp^2 hybridization of carbon). The G band at 1320 cm^{-1} corresponds to polycrystalline graphite [61]. Absorption in the regions around 1200 and 1490 cm^{-1} is attributed to non-planar fragments containing carbon atoms in sp^3 hybridization [61]. The depth of the “gap” between lines D and G can be used to estimate the perfection of the graphite structure responsible for electronic conductivity of the carbon coating. The ratio of integral intensities of lines corresponding to carbon in sp^2 and sp^3 hybridization

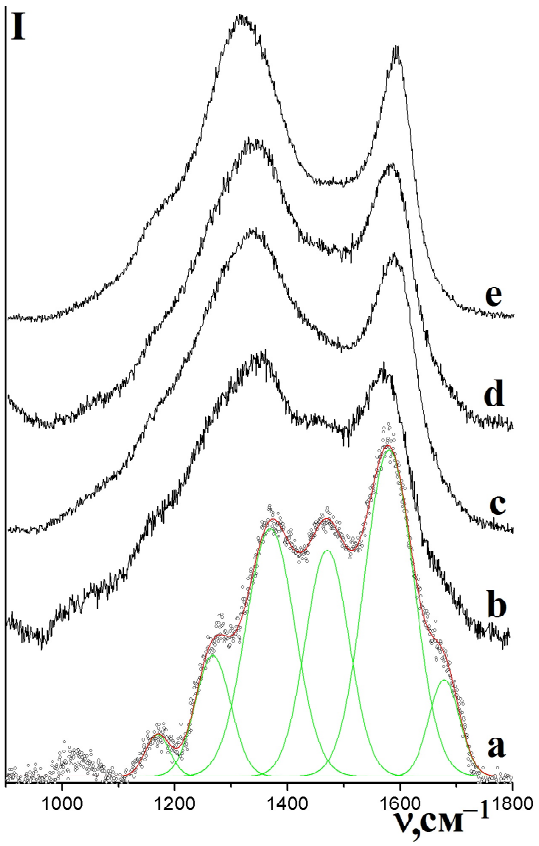

Fig. 4. Raman spectra in the range of 900-1800 cm^{-1} for the samples calcined at 400 °C in air followed by calcination in an inert atmosphere at 400 (a), 600 °C (c) with sucrose addition and at 400 (b), 600 (d) and 800 °C (e) without sucrose addition. Decomposition into components is shown for the spectrum (a).

(degree of graphitization) increases with an increase in temperature, and a sample obtained in the inert atmosphere at 800 °C manifests a spectrum characteristic of a well formed graphite with an additional line near 1080 cm^{-1} (Fig. 4e). It should also be noted that a somewhat less perfect graphite phase is formed at the same treatment temperature in samples obtained by calcination after sucrose addition (Figs. 4a-4d).

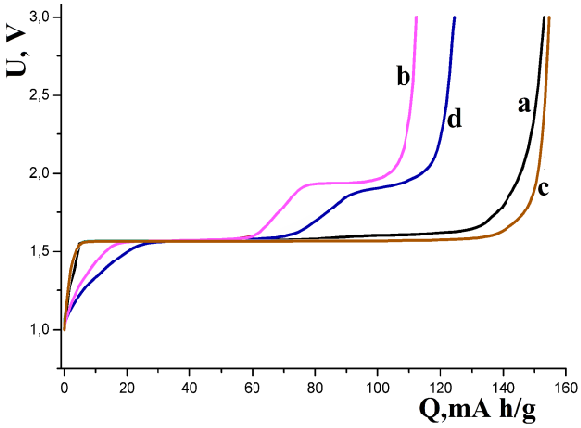

Fig. 5. Charge-discharge curves of the 5th cycle for samples calcined in air at 800 °C (a), in the inert atmosphere at 600 (b) and 800 °C (c) without sucrose addition, as well as at 600 °C (d) with sucrose addition. Current density: 20 mA/g.

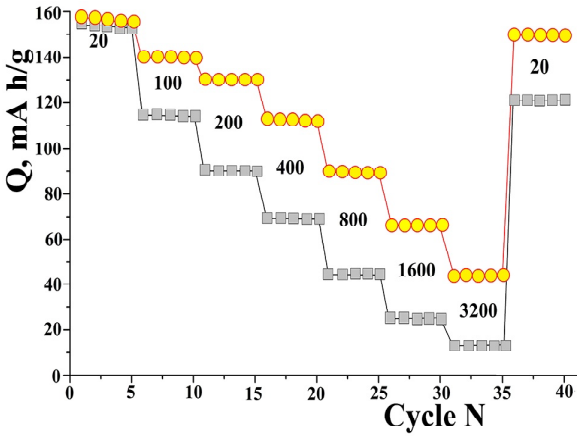

Fig. 6. Cycling performance of samples calcined at 800 °C in air (à) and in the inert atmosphere (b). The current densities are shown in the Figure.

During the first charging cycle, all the materials studied are characterized by rather high irreversible capacity due to electrolyte reduction. Its value is the higher, the smaller the particle size in the samples (the lower the calcination temperature). Its value is the largest for the samples obtained at 400 °C and the smallest for the samples obtained at 800 °C. The irreversible capacity decreases quickly during cycling.

The charge and discharge of samples calcined at 800 °C in a wide range of degree of lithium intercalation occurs at a nearly constant potential of about 1.55 V (Fig. 5). The charge-discharge curves of samples obtained at 600 °C contain one more plateau at 1.8 V corresponding to lithium intercalation into anatase [60]. The capacity of samples obtained at 600 °C with sucrose addition is higher than that of samples obtained at the same temperature without sucrose addition. This is caused by a smaller particle size in both phases (anatase and lithium titanate) in case of sucrose addition.

The discharge capacity of materials calcined in air and argon at 800 °C was nearly the same and equaled 155 mAh/g at 20 mA/g. However, in a sample calcined in air that has no carbon coating, this value decreases quickly upon cycling at high current rates (Fig. 6). The capacity was about three times higher for 3200 mAh/g current density (charge rate *ca*. 20 C), or two times higher for 1600 mAh/g current density (charge rate *ca*. 10 C), than that of a sample calcined in argon. Thus, formation of a carbon coating results in a smaller capacity decrease at high current densities. Samples obtained at 800 °C in the inert atmosphere show good cyclic performance (the capacity retention of the first cycle is about 80%). Furthermore, their capacity returns to original values on transition from high to small currents (Fig. 6).

7. CONCLUSION

Based on literature review in the field of anode materials based on silicon, tin, titanium oxides, and lithium titanate for lithium-ion cells, it can be concluded that formation of nanocomposites with carbon makes it possible to stabilize these materials and their capacity during cycling. The treatment temperature and carbon precursor affect considerably the formation of particles, including their size, and the electrochemical properties of the resulting composite materials with carbon.

ACKNOWLEDGEMENTS

This study was financially supported by the Russian scientific foundation, Project no. 16-29-05241.

REFERENCES

[1] B. Scrosati and J. Garche // *J. Power Sources* **195** (2010) 2419.
[2] V. Etacheri, R. Marom, R. Elazari, G. Salitra and D. Aurbach // *Energy Environ. Sci.* **4** (2011) 3243.
[3] A.B. Yaroslavtsev, T.L. Kulova and A.M. Skundin // *Russ. Chem. Rev*. **84** (2015) 826.

[4] G. Maurin, Ch. Bousquet, F. Henn, P. Bernier, R. Almairac and B. Simon // *Solid State Ionics* **136-137** (2000) 1295.
[5] B.S. Bokstein and A.B. Yaroslavtsev, *Diffusin of atoms and ions in solids* (MISIS Press, Moscow, 2005).
[6] X. Xiang, Z. Huang, E. Liu, H. Shen, Y. Tian, H. Xie, Y. Wu and Z. Wu // *Electrochim. Acta* **56** (2011) 9350.
[7] D. Zhang, Y. Zhao, J.B. Goodenough, Y. Lu, Ch. Chen, L. Wang and J. Liu // *Electrochem. Comm.* **13** (2011) 125.
[8] Ch. Kang, I. Lahiri, R. Baskaran, W.-G. Kim, Y.-K. Sun and W. Choi // *J. Power Sources* **219** (2012) 364.
[9] S. Klink, E. Ventosa, W. Xia, F. La Mantia, M. Muhler and W. Schuhmann // *Electrochem. Comm.* **15** (2012) 10.
[10] Ch.de las Casas and W. Li // *J. Power Sources* **208** (2012) 74.
[11] J.C. Withers, R.O. Loutfy and T.P. Lowe // *Fullerene Sci. Technol.* **5** (1997) 1.
[12] A.S. Claye, J.E. Fischer, C.B. Huffman, A.G. Rinzler and R.E. Smalley // *J. Electrochem. Soc.* **147** (2000) 2845.
[13] L.H. Huang, Z.H. Min and Q.Y. Zhang // *Rev. Adv. Mater. Sci.* **36** (2014) 13.
[14] W.-J.Zhang // *J. Power Sources* **196** (2011) 13.
[15] J.H. Ryu, J.W. Kim, Y.-E. Sung and S.M. Oh // *Electrochem. Solid-State Lett*. **7** (2004) A306.
[16] S. Bourderau, T. Brousse and D.M. Schleich // *J. Power Sources* **81-82** (1999) 233.
[17] A. Netz, R.A. Huggins and W. Weppner // *J. Power Sources* **119-121** (2003) 95.
[18] U. Kasavajjula, C. Wang and A.J. Appleby // *J. Power Sources* **163** (2007) 1003.
[19] T.L. Kulova, A.M. Skundin, Yu.V. Pleskov, E.I. Terukov and O.I. Kon'kov // *J. Electroanalyt. Chem.* **600** (2007) 217.
[20] Sh. Ohara, Ju. Suzuki, K. Sekine and T. Takamura // *J. Power Sources* **119-121** (2003) 591.
[21] K. K. Yoshimura, Ju. Suzuki, K. Sekine and Ts. Takamura // *J. Power Sources* **146** (2005) 445.
[22] L. Shen, X. Guo, X. Fang, Zh. Wang and L. Chen // *J. Power Sources* **213** (2012) 229.
[23] Sh. Iwamura, H. Nishihara and T. Kyotani // *J. Power Sources* **222** (2013) 400.
[24] M. Thakur, M. Isaacson, S.L. Sinsabaugh, M.S. Wong and S.L. Biswal // *J. Power Sources* **205** (2012) 426.
[25] Y. He, X. Yu, G. Li, R. Wang, H. Li, Y. Wang, H. Gao and X. Huang // *J. Power Sources* **216** (2012) 131.
[26] G.V. Li, T.L. Kulova, V.A. Tolmachev, A.V. Chernienko, M.A. Baranov, S.I. Pavlov, E.V. Astrova and A.M. Skundin // *Semiconductors* **47** (2013) 1288.
[27] J.-H. Cho, X. Li and S.T. Picraux // *J. Power Sources* **205** (2012) 467.
[28] V. Chakrapani, F. Rusli, M.A. Filler and P.A. Kohl // *J. Power Sources* **205** (2012) 433.
[29] L.-F. Cui, R. Ruffo, C.K. Chan, H. Peng and Y. Cui // *Nano Letters* **9** (2009) 491.
[30] K. Zhao, M. Pharr, L. Hartle, J.J. Vlassak and Z. Suo // *J. Power Sources* **218** (2012) 6.
[31] H. Kim, M. Seo, M.-H. Park and J. Cho // *Angew. Chem. Int. Ed.* **49** (2010) 2146.
[32] C. Lupu, J.-G. Mao, J.W. Rabalais, A.M. Guloy and J.W. Richardson // *Inorg. Chem*. **42** (2003) 3765.
[33] J. Chen // *Materials* **6** (2013) 156.
[34] J.O. Besenhard, J. Yang and M. Winter // *J. Power Sources* **68** (1997) 87.
[35] J.-H. Kim, S. Khanal, M. Islam, A. Khatri and D. Choi // *Electrochem. Comm.* **10** (2008) 1688.
[36] A.R. Kamali and D.J. Fray // *Rev. Adv. Mater. Sci.* **27** (2011) 14.
[37] X.-L. Wang, M. Feygenson, H. Chen, C.-H. Lin, W. Ku, J. Bai, M.C. Aronson, T.A. Tyson and W.-Q. Han // *J. Am. Chem. Soc*. **133** (2011) 11213.
[38] M. Wachtler, M. Winter and J.O. Besenhard // *J. Power Sources* **105** (2002) 151.
[39] X.-Y. Fan, F.-S. Ke, W. Guo-Zhen, H. Ling and S.-G. Sun // *Electrochem. Solid-State Lett.* **11** (2008) A195.
[40] R.Z. Hu, M.Q. Zeng and M. Zhu // *Electrochim. Acta* **54** (2009) 2843.
[41] M.-S. Wang, L.-Zh. Fan, M. Huang, J. Li and X. Qu // *J. Power Sources* **219** (2012) 29.
[42] Q. Sa and Y. Wang // *J. Power Sources* **208** (2012) 46.
[43] Q. Si, M. Matsui, T. Horiba, O. Yamamoto, Y. Takeda, N. Seki and N. Imanishi // *J. Power Sources* **241** (2013) 744.
[44] W. Li, R.Yang, X. Wang, T. Wang, J. Zheng and X. Li // *J. Power Sources* **221** (2013) 242.
[45] B.-C. Yu, Y. Hwa, J.-H. Kim and H.-J. Sohn // *Electrochem. Comm*. **46** (2014) 144.

[46] C.S. Wang, G.T. Wu, X.B. Zhang, Z.F. Qi and W.Z. Li // J. *Electrochem. Soc.* **145** (1998) 2751.
[47] A. Magasinski, P. Dixon, B. Hertzberg, A. Kvit, J. Ayala and G. Yushin // *Nat. Mater.* **9** (2010) 353.
[48] J.K. Lee, K.B. Smith, C.M. Hayner and H.H. Kung // *Chem. Commun*. **46** (2010) 2025.
[49] J. Luo, X. Zhao, J. Wu, H.D. Jang, H.H. Kung and J. Huang // *J. Phys. Chem. Lett.* **3** (2012) 1824.
[50] W. Wang and P.N. Kumta // *J. Power Sources* **172** (2007) 650.
[51] T.L. Kulova and A.M. Skundin // *Russ. J. Electrochem.* **48** (2012) 330.
[52] J. Hassoun, S. Panero, P. Simon, P.L. Taberna and B. Scrosati // *Adv. Mater.* **19** (2007) 1632.
[53] R. Zhang and M.S. Whittingham // *Electrochem. Solid-State Lett.* **13** (2010) A184.
[54] B. Luo, B. Wang, M. Liang, J. Ning, X. Li and L. Zhi // *Adv. Mater.* **24** (2012) 1405.
[55] I.N. Markova, Olivier Chauvet, T.I. Petrov, V.P. Stefanova, I.D. Denev and S.A. Uzunova // *Rev. Adv. Mater. Sci.* **35** (2013) 59.
[56] V.L. Milanova, M.B. Piskin, T.I. Petrov, T.E. Stankulov, I.D. Denev and I.N. Markova // *Rev. Adv. Mater. Sci.* **41** (2015) 52.
[57] W.Zhenyao, C.Ge and X.Dingguo // *J. Power Sources* **184** (2008) 432.
[58] S. Yang, H. Song, H. Yi, W. Liu, H. Zhang and X .Chen // *Electrochim. Acta* **55** (2009) 521.
[59] Z.G.Yang, D.Choi, S.Kerisit, K.M.Rosso, D.H.Wang, J.Zhang, G.Graff and J.Liu // *J. Power Sources* **192** (2009) 588.
[60] U.Lafont, D.Carta, G.Mountjoy, A.V.Chadwick and E.M.Kelder // *J. Phys. Chem. C* **114** (2010) 1372.
[61] R.Baddour-Hadjean and J.P.Pereira-Ramos // *Chem. Rev*. **110** (2010) 1278.
[62] W.J.H. Borghols, M. Wagemaker, U. Lafont, E.M. Kelder and F.M. Mulder // *Chem. Mater.* **20** (2008) 2949.
[63] G.Sudant, E. Baudrin, D. Larcher and J.M. Tarascon // *J. Mater.Chem*. **15** (2005) 1263.
[64] M. Mancini, P. Kubiak, J. Geserick, R. Marassi, N. Husing and M. Wohlfahrt-Mehrens // *J. Power Sources* **189** (2009) 585.
[65] Y. Wang, X.W. Su and S. Lu // *J. Mater. Chem.* **22** (2012) 1969.
[66] A. Moretti, G.T. Kim, D. Bresser, K. Renger, E. Paillard, R. Marassi, M. Winter and S. Passerini // *J. Power Sources* **221** (2013) 419.
[67] P. Zhu, Y. Wu, M.V. Reddy, A.S. Nair, B.V.R. Chowdari and S. Ramakrishna // *RSC Adv.* **2** (2012) 531.
[68] S.B. Yang, X.L. Feng and K. Mullen // *Adv. Mater*. **23** (2011) 3575.
[69] B. Zhao, R. Cai, S. Jiang, Y. Sha and Z. Shao // *Electrochim. Acta* **85** (2012) 636.
[70] M. Marinaro, M. Pfanzelt, P. Kubiak, R. Marassi and M. Wohlfahrt-Mehrens // *J. Power Sources* **196** (2011) 9825.
[71] K. Zaghib, M. Simoneau, M. Armand and M. Gauthier // *J. Power Sources* **81-82** (1999) 300.
[72] J. Lu, C. Nan, Q. Peng and Y. Li // *J. Power Sources* **202** (2012) 246.
[73] D.V. Safronov, S.A. Novikova, A.M. Skundin and A.B. Yaroslavtsev // I*norg. Mater.* **48** (2012) 57.
[74] S. Schamer, *W. Weppner and P.* Schmid-Beurmann // *J. Electrochem. Soc*. **146** (1999) 857.
[75] M. Wilkening, R. Amade, W. Iwaniak and P. Heitjans // *Phys. Chem. Chem. Phys*. **9** (2007) 1239.
[76] T.F. Yi, L.J. Jiang, J. Shu, C.B. Yue, R.S. Zhu and H.B. Qiao // *J. Phys. Chem. Solids* **71** (2010) 1236.
[77] A. Nugroho, S.J. Kim, K.Y. Chung and J. Kim // *Electrochim. Acta* **78** (2012) 623.
[78] L.J. Xi, H.K. Wang, S.L. Yang, R.G. Ma, Zh.G. Lu, Ch.W. Cao, K.L. Leung, J.Q. Deng, A.L. Rogach and C.Y. Chung // *J. Power Sources* **242** (2013) 222.
[79] C. Zhang, Y. Zhang, J. Wang, D. Wang, D. He and Y. Xia // *J. Power Sources* **236** (2013) 118.
[80] C. Lai, Z.Z. Wu, Y.X. Zhu, Q.D. Wu, L. Li and Ch. Wang // *J. Power Sources* **226** (2013) 71.
[81] Sh. Huang, Zh. Wen, J. Zhang, Zh. Gu and X. Xu // *Solid State Ionics* **177** (2006) 851.
[82] H. Yu, X. Zhang, A.F. Jalbout, X. Yan, X. Pan, H. Xie and R. Wang // *Electrochimica Acta* **53** (2008) 4200.
[83] X. Li, M. Qu, Y. Huai and Z. Yu // *Electrochim. Acta* **55** (2010) 2978.
[84] Y. Shi, L. Wen, F. Li and H.-M. Cheng // *J. Power Sources* **196** (2011) 8610.

[85] Y.B. He, F. Ning, B.H. Li, Q.S. Song, W. Lv, H.D. Du, D.Y. Zhai, F.Y. Su, Q.H. Yang and F.Y. Kang // *J. Power Sources* **202** (2012) 253.
[86] H. Zhang, Q. Deng, Ch. Mou, Z. Huang, Y. Wang, A. Zhou and J. Li // *J. Power Sources* **239** (2013) 538.
[87] H. Li, L. Shen, X. Zhang, J. Wang, P. Nie, Q. Che and B. Ding // *J. Power Sources* **221** (2013) 122.
[88] H. Luo, L. Shen, K. Rui, H. Li and X. Zhang // *J.Alloys Compounds* **572** (2013) 37.
[89] T. Yuan, X. Yu, R. Cai, Y. Zhou and Z. Shao // *J. Power Sources* **195** (2010) 4997.
[90] X. Hu, Z. Lin, K. Yang, Y. Huai and Zh. Deng // *Electrochimica Acta* **56** (2011) 5046.
[91] Y. Ren, X. Huang, H. Wang, J. Ding, Sh. Zhou, Y. Chen, B. Liu and X. Zeng // *Ionics* **21** (2015) 629.
[92] H. Xu, X. Hu, W. Luo, Y. Sun, Z. Yang, Ch. Hu and Y. Huang // *Chem. Elecrochem.* **1** (2014) 611.
[93] L. Cheng, X.-L. Li, H.-J. Liu, H.-M. Xiong, P.-W. Zhang and Y.-Y. Xia // *J. Electrochem. Soc.* **154** (2007) A692.
[94] L. Cheng, J. Yan, G.-N. Zhu, J.-Y. Luo, C.-X. Wang and Y.-Y. Xia // *J. Mater. Chem.* **20** (2010) 595.
[95] X. Li, M. Qu, Y. Hua and Z. Yu // *Electrochimica Acta* **55** (2010) 2978.
[96] T. Li, L. Shao, X. Lin, M. Shui, K. Wu, D. Wang, N. Long, Y. Ren and J. Shu // *J. Electroanal. Chem.* **722–723** (2014) 54.
[97] Y. Zhang, X. Hu, Y. Xu and Ch. Chen // *Solid State Ionics* **276** (2015) 18.